



Effect of Multiwalled Carbon Nanotube Contents on Photophysical Properties of Poly-TPD/MWCNT Nanocomposites

Bandar Ali Al-Asbahi¹

Received: 12 March 2023 / Accepted: 6 May 2023 / Published online: 16 May 2023
© The Author(s), under exclusive licence to Springer Science+Business Media, LLC, part of Springer Nature 2023

Abstract

Tuning photophysical properties of poly[bis(4-butyphenyl)-bis(phenyl)benzidine] (poly-TPD) by addition multi walled carbon nanotubes (MWCNTs) with different weight ratios is demonstrated. The solution blending method followed by spin coating technique was used to successfully prepare thin films of poly-TPD/MWCNTs. Fourier transform infrared spectroscopy (FTIR) revealed the interaction between poly-TPD and MWCNT. UV–Vis and photoluminescence spectrophotometer were used to determine the optical properties. No chemical interaction was detected between poly-TPD and MWCNTs in their ground states, as evidenced by the absence of new peaks in FTIR and absorption spectra. The nanocomposites showed reduced direct (E_{gd}) and indirect (E_{gi}) energy band gaps values, while Urbach energy (E_u) values increased with increasing MWCNT doping, resulting in a narrower optical energy band gap width and an increase in localized energy levels that act as electron traps in the band gap. The charge transfer from poly-TPD to MWCNTs was evidenced by the reduction in poly-TPD emission, as well as changes in both the values of Stokes shift and vibronic spacing energy in the nanocomposite system. The parameters of the Stern–Volmer quenching constant (k_{SV}), fluorescence lifetime (τ) of excited poly-TPD in the presence of MWCNTs, photo-induced electron-transfer rate (k_{ET}), and bimolecular quenching rate (k_q) can be adjusted to further enhance efficient charge transfer between poly-TPD and MWCNTs.

Keywords Photophysical properties · Poly-TPD/MWCNTs nanocomposite · Charge transfer

1 Introduction

The recent surge in interest in scientific and industrial societies for the fabrication of nanocomposites is due to their desirable characteristics, such as multi-functional capabilities, multifaceted, low cost, low weight, ease-of-synthesis, and improved thermal, optical, and optoelectronic properties [1, 2]. These nanocomposites are used in optical and optoelectronic devices as well as dielectric materials to create capacitors with improved dielectric permittivity and refractive index [3, 4]. To take advantage of these nanocomposite features it is necessary to adjust the optoelectronic characteristics through a suitable selection of ionic fillers and optimal filler loadings with charge-relocation exchanges between the organic material and the incorporated ions, often resulting

in increased concentrations and consequently enhanced refractive index. The need for polymers with a high index of refraction to have excellent photosensitive clarity has attracted much attention [5] due to its potential applications in optoelectronic devices such as OLED devices [6], substrates for advanced display devices [7], photoresistors [8], antireflection optical coatings [9], and microlenses for charge-coupled devices or metal-oxide-semiconductors [10]. However, the implementation of nanofillers often results in a decrease in transparency due to the disruption of ionic agglomeration [11].

Since their discovery in 1991, carbon nanotubes (CNTs) have been seen by researchers as a key material for the nanotechnology revolution of the twenty first century. The enthusiasm for CNTs is due to their remarkable properties; they possess special electronic, chemical, thermal and mechanical characteristics, have low mass density, are highly flexible and boast an extremely high surface area. Furthermore, they have a large aspect ratio and can create a huge interface in polymer nanocomposites [12–15]. These qualities have led to interest in using CNTs as fillers in polymer composite systems

✉ Bandar Ali Al-Asbahi
balasbahi@ksu.edu.sa

¹ Department of Physics & Astronomy, College of Science, King Saud University, P.O. Box 2455, Riyadh 11451, Saudi Arabia

to create ultra-light structural materials with improved electrical, thermal and optical features [16]. In the last decade, the development of new materials, particularly polymer/CNT composites, has become a topic of great interest. However, further research is needed to improve their physical properties and to create potential applications [17]. The optical properties of CNT arrays are based on the atomic structure of each individual CNT and how they are arranged collectively. Single walled carbon nanotubes (SWCNTs) and multi walled carbon nanotubes (MWCNTs) have different optical properties due to their size. Since MWCNTs are larger, they have more uniform optical properties [18] which can be treated as a homogeneous medium for various applications [19].

The purpose of incorporating CNTs into polymers is due to their unique optoelectronic, electronic, and electrical properties, as well as the potential for a variety of interfacial configurations in the nanocomposite [12, 15]. Kumar et al. [14] studied MWCNTs in polyaniline to boost its optoelectrical conductivity and bolster its electromagnetic interference protection. Additionally, Kim et al. [20] looked into the polymethylmethacrylate (PMMA) doped with MWCNTs to prevent microbial growth issues. Hazem et al. [21] determined that the addition of MWCNTs to spinel ferrites made it a possible choice for optoelectronic devices and capacitive storage. Morsi et al. [22] found that the combination of MWCNTs/Au filler with polyethylene oxide matrix improved the electrical, thermal and optical properties of organoelectronic devices.

One of the most investigated conjugated polymers in most optoelectronic devices is poly[bis(4-butyphenyl)-bis(phenyl)benzidine] (abbreviated as poly-TPD). In the current work, the optoelectronic properties of poly-TPD/MWCNTs composite in various weight ratios prepared by solution blending method, have been studied. Despite many researches on the optical and optoelectronic properties improvement of polymers upon incorporating MWCNTs [12, 13, 23–25], there have been no studies presented the MWCNTs effects on the poly-TPD properties. This paper investigates the effects of MWCNTs on the structural and optoelectronic properties of poly-TPD. To do this, XRD patterns, FTIR spectra, absorption and emission spectra were used to analyze the poly-TPD and poly-TPD/MWCNTs composites. Additionally, parameters such as the Stern–Volmer quenching constant (k_{SV}), fluorescence lifetime (τ) of excited poly-TPD in the presence of MWCNTs, photo-induced electron-transfer rate (k_{ET}), and bimolecular quenching rate (k_q) were determined to evaluate the charge transfer between the poly-TPD and MWCNTs.

2 Materials and Methods

Poly-TPD, with molecular weight of 15,000 g/mole, and MWCNTs with outer diameter ~5–20 nm and length of 1.0 μm , were purchased from American Dye Source, Inc.

(Baie d’Urfé, Quebec, Canada) and Chargen Life Sciences LLP (NS Phadke Marg, Mumbai, India), respectively. Poly-TPD was dissolved in toluene by sonicated for 1 h to obtain homogenous liquid and the MWCNTs powder was dispersed into toluene by sonicated for 5 h. MWCNTs with various weight ratios (0.5, 1.0, 1.5, 2.0, 2.5, 3.0, 5.0 and 10 wt%) were added to fixed toluene solution of poly-TPD (1.0 mg/ml) by solution blending method under sonication for 2 h to get homogenous specimens. Special quartz cuvette with optical length of 1.0 mm was used for characterization all the samples.

The structural properties of the all specimens were investigated by X-ray diffraction (XRD; Miniflex 600, Rigaku, Japan), Fourier transform infrared spectroscopy (FT-IR; PerkinElmer Spectrum 100, Connecticut, USA), and Transmission electron microscopy (TEM; JEOL JEM-1400, Tokyo, Japan) techniques. The optical properties of all the samples were investigated from the obtained absorption and emission spectra, which collected by UV–Vis spectrophotometer (JASCO V-670, Cremella, Italia) and spectrofluorometer (JASCO FP-8200, Cremella, Italia), respectively.

3 Results and Discussion

The FTIR spectroscopy was used to analyze the interaction between poly-TPD and MWCNT. The FTIR spectra of poly-TPD, MWCNT and poly-TPD/MWCNTs in Fig. 1 demonstrate the formation of the nanocomposite. The broad band at 3440 cm^{-1} in all samples is attributed to the stretching mode of O–H absorbed by the samples [25, 26]. The FTIR results also show that the aromatic C–H stretching (weak) at 3059 cm^{-1} for poly-TPD is present in the composites as well. Moreover, a shift by 30 cm^{-1} to 3029 cm^{-1} was observed in both composites with 2.5 and 5.0 wt% MWCNT for the

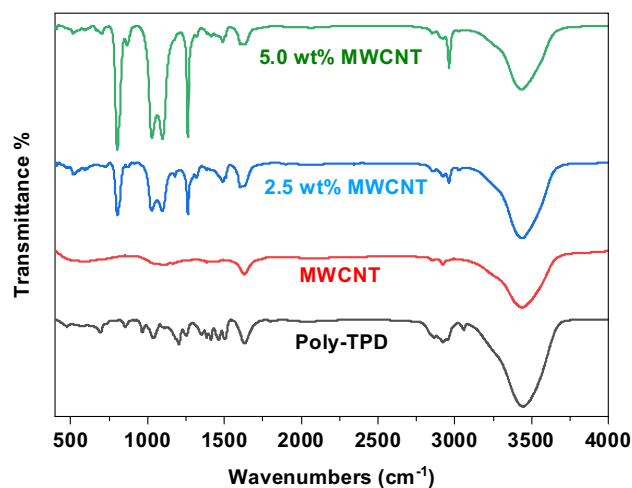


Fig. 1 FTIR spectra of poly-TPD, MWCNT, and their composites

aromatic C–H out-of-plane stretch. Additionally, bands at 2860–2960 cm^{-1} are assigned to the stretching vibrations of $-\text{CH}_2-$ and $-\text{CH}_3-$ groups and also to the microstructure formation of the specimen [27]. The peak at 1630 cm^{-1} in the transmittance spectrum of MWCNT is due to the C=C stretching vibration of the graphite structure in the MWCNT framework [28]. The 1507 cm^{-1} and 1630 cm^{-1} peaks are attributed to the C=C stretching of the aromatic structure from poly-TPD, and 695 cm^{-1} is a characteristic of the benzene ring. The 1265 cm^{-1} peak in poly-TPD and poly-TPD/MWCNT composites is assigned to C–N stretch band of aromatic amine. Additionally, peak from C–O–C stretching is observed at 1112 cm^{-1} in MWCNTs and both composites with 2.5 wt% and 5.0 wt% MWCNT content. Lastly, the bands at 957 cm^{-1} and 855 cm^{-1} are associated with trans double bond vinylene C–H wagging and phenyl C–H wagging, respectively, which indicates a dipole normal to the phenyl vinyl plane [29, 30]. The peak positions, linewidths, and intensities of the vibrations have been altered by the introduction of MWCNTs into poly-TPD, which implies that MWCNTs have been incorporated into the poly-TPD matrix. The significant changes in linewidth and intensity of the vibrational bands are likely due to the high electronegativity of MWCNTs, which has a major effect on the frequency spectrum of nearby groups [31].

Figure 2 shows the absorption spectra of the solution of poly-TPD with various incorporation of MWCNTs. A broad absorption band at 366 nm was seen in the pristine poly-TPD due to the $\pi-\pi^*$ transition of the conjugated polymer. With an increase in MWCNTs, the absorbance of the poly-TPD was increased with a longer absorption tail which would be beneficial for light harvesting in the visible region. No significant wavelength shift or extra peaks were observed, suggesting that there is no chemical interaction between poly-TPD and MWCNTs at ground states [26, 32]. A slight change in intensity of absorption band between pristine poly-TPD and poly-TPD/MWCNT composites can be attributed to good quality dispersion of MWCNTs in the polymer matrix. The MWCNTs act as a photon scattering centers in the nanocomposite. By increasing the amount of MWCNT, more photons are captured by nanocomposite structures, thus resulting in higher absorbance values.

The optical energy band gap (E_g) between the valance band and the conduction is a key factor in determining the potential use and performance of organic and inorganic materials in optoelectronic applications. The UV–VIS absorption spectra of composites can be used to detect changes in the band structure and to calculate E_g . The Tauc method is commonly used for this purpose, which involves the equation [33]:

$$\alpha h\nu = B(h\nu - E_g)^m \quad (1)$$

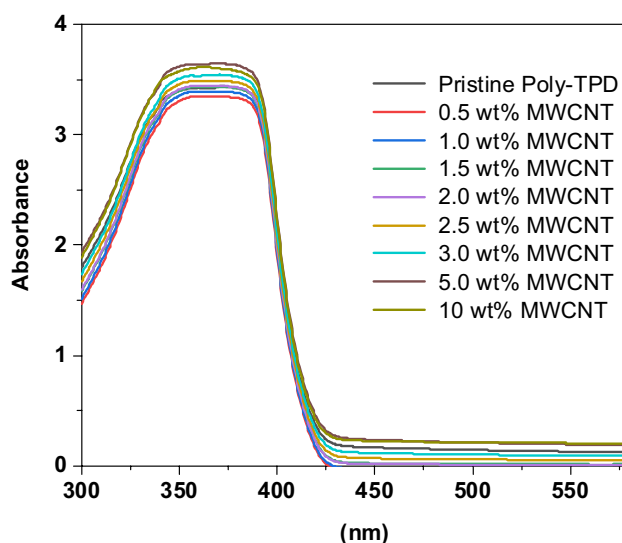


Fig. 2 Absorption spectra of pristine poly-TPD and poly-TPD/MWCNT composites

where α is the absorption coefficient, $(h\nu)$ is the photon energy, B is a constant, and m is a parameter that gives the type of electron transition. This equation defines direct allowed transitions for $m = 1/2$ and indirect allowed transitions for $m = 2$; these are illustrated in Fig. 3a, b. The linear regions on the right-hand side of both graphs indicate that the direct (E_{gd}) and indirect (E_{gi}) allowed transition band gap energies of poly-TPD/MWCNT composite can be calculated. The E_{gd} and E_{gi} optical band gap energies were determined from the cut-off point at the $(h\nu)$ -axis of the linear straight lines in Fig. 3a, b, as shown in Table 1. The existence both types of band gaps in poly-TPD/MWCNT composite implies that the absorption energy range can be extended to enhance photoelectric energy conversion [34]. It is evident that an increase in MWCNT content leads to a slight decrease in both E_{gd} and E_{gi} of poly-TPD. This is due to a slight increase in the localized energy levels acting as electron traps in the band gap, thus reducing the gap between conduction and valance bands [35].

The Urbach energy (Band tail) can be used to determine if a sample is crystalline or amorphous after doping [36, 37]. The optical absorption coefficient (α) near the edge of the band typically follows an exponential relationship given by Urbach [38], which is expressed as:

$$\alpha = \alpha_0 \exp(h\nu/E_u) \quad (2)$$

Here, α_0 is a constant, $(h\nu)$ is the photon energy and E_u is the band tail energy of localized states in the forbidden band gap. This energy is associated with the amorphous nature of the material and reflects the width of the Urbach tail due to defects in the forbidden band gap between valance

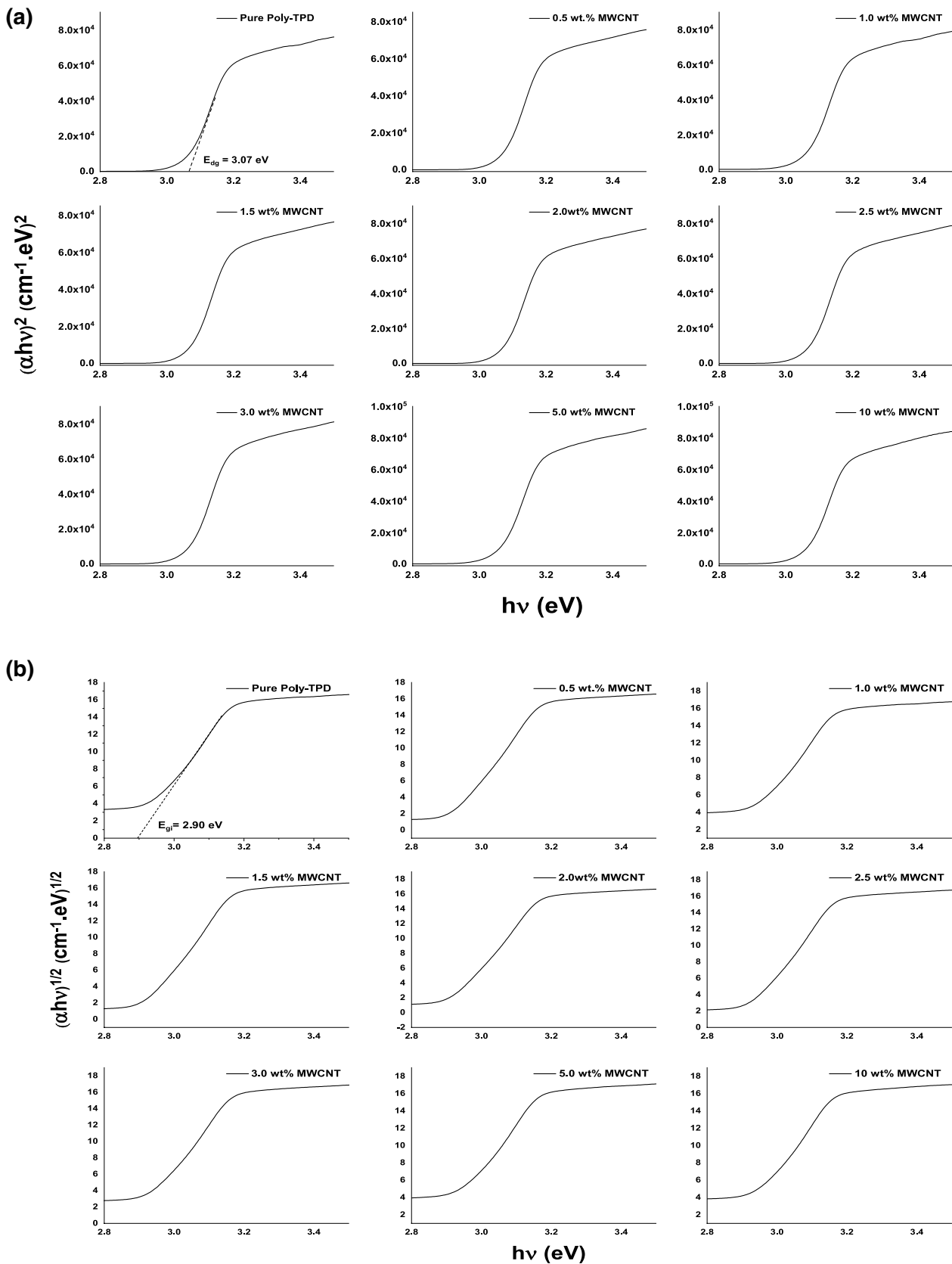


Fig. 3 a Direct band gap and b indirect band gap for nanocomposites with various poly-TPD/MWCNTs weight ratio

and conduction bands. The inverse slope of $\ln\alpha-(h\nu)$ graph according to Eq. (2) gives an indication of Urbach energy. Figure 4 shows how $\ln\alpha$ values change according to $(h\nu)$ for poly-TPD/MWCNT composites. The values of E_u , which are lower than the energy band gap, were determined by the slope of the straight lines in Fig. 4 and listed in Table 1. As the MWCNT content increases, the E_u values also increase exponentially. The decrease in Urbach energy indicates an increase in the crystalline region while an increase in Urbach energy implies a rise in the amorphous part [36, 37]. This means that as MWCNT doping increases, the nanocomposite system becomes more amorphous. Examining Table 1 again reveals that both E_{gd} and E_{gi} values of nanocomposites are reduced with increasing E_u values. The addition of MWCNTs to poly-TPD alters the width of localized states within the optical band gap. The rise in E_u suggests that defects within nanocomposites are increased due to MWCNT doping, thus leading to a decrease in optical energy band gap width [39].

The steepness parameter (σ) that described the broadening/shrinkage of optical absorption edge can be altered due

Table 1 Optical properties of pristine poly-TPD and poly-TPD/MWCNT composite

Content of MWCNT wt%	E_{gd} (eV)	E_{gi} (eV)	n	E_u (meV)	$\sigma \times 10^{-2}$
0	3.07	2.90	1.803	75.88	34.26
0.5	3.07	2.88	1.808	74.73	34.79
1.0	3.07	2.89	1.805	76.02	34.19
1.5	3.07	2.90	1.803	76.78	33.86
2.0	3.07	2.90	1.803	76.26	34.09
2.5	3.07	2.90	1.803	79.97	32.51
3.0	3.07	2.88	1.808	83.60	31.09
5.0	3.06	2.87	1.811	88.18	29.48
10	3.06	2.86	1.813	89.51	29.04

to interactions of the electron-phonon or exciton-phonon. As seen in Table 1, a decrease in σ or an increase in E_u is observed when MWCNTs are added, which is attributed to the increased localized density of electronic states within the forbidden band gap of the composites and thus higher

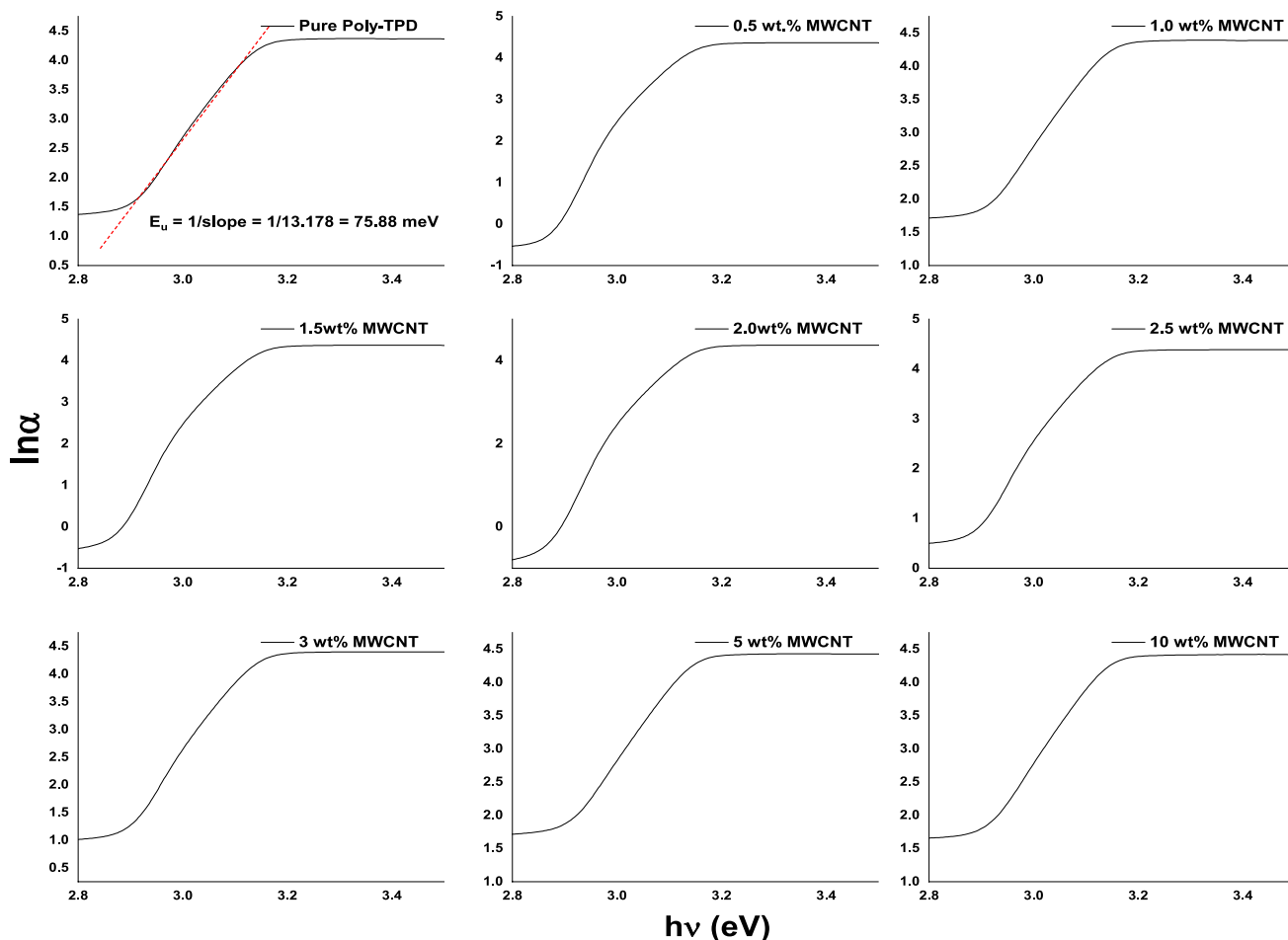


Fig. 4 Urbach energy for the poly-TPD with various MWCNTs weight ratio

disorder degree in the electronic structure of the nanocomposite [40, 41].

Equation (3) can be used to calculate the refractive index (n) as a function of E_g for poly-TPD/MWCNT composites [42, 43]:

$$\frac{n^2 - 1}{n^2 + 2} = 1 - \sqrt{\frac{E_g}{20}} \quad (3)$$

where n is the linear refractive index for λ_g corresponding to the E_g . As the MWCNT content increases, the number of scattering centers in the composite rises and light circulates more in the material. This leads to a decrease in the light speed that passing through the composite ($n = c/v$) and an increase in n values, as seen in Table 1. This increase in n values makes these poly-TPD/MWCNT composites a promising candidate for coatings and optoelectronic applications.

Figure 5 illustrates the photoluminescence spectra of poly-TPD with various amounts of MWCNTs when exposed at a 350 nm excitation wavelength. The absorbed radiation energizes the electrons from their ground state, and when they return to the ground state, they emit energy radiation equivalent to the optical bandgap of the material. The primary peak in the emission spectrum of pristine poly-TPD at 419 nm (Near Band edge emission–NBE) is a result of the relaxation of excited π -electrons to their ground state (0–0 vibronic band transition), while the shoulder peaks at 440 and 468 nm are related to interchange states (0–1 and 0–2 vibronic band transitions, respectively). The peaks at 419 nm and 440 nm indicate violet emission, while the shoulder at 468 nm corresponds to blue emission. It is evident that the

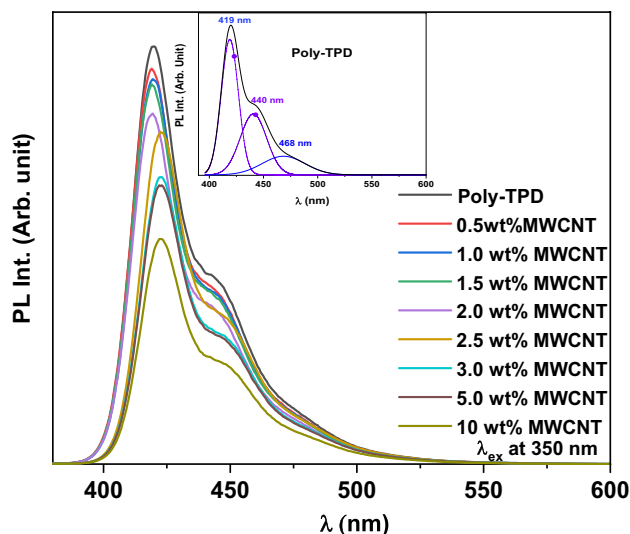


Fig. 5 Emission spectra of the pristine poly-TPD deposited with various MWCNTs weight ratio at excitation wavelength of 350 nm. The inset is the deconvoluted emission curve of poly-TPD by Gaussian fitting

emission intensities of all peaks were reduced with the addition of MWCNTs and then shifted to a higher wavelength at high content (≥ 2.5 wt%). The decrease in poly-TPD emission in the composite system was caused by charge transfer from poly-TPD to MWCNTs. This inhibited recombination of excitons in poly-TPD, causing electrons to move across the interface into MWCNTs while holes remain in the poly-TPD. The red shift in the PL spectra is due to an increase in poly-TPD conjugation length [44]. The presence of MWCNTs causes separation between polymer chains, resulting in a change in conjugation length and thus a red shift in the PL spectra. The proposed photocatalysis mechanism in the poly-TPD/MWCNT nanocomposite can involve several steps. Upon exposure to light, poly-TPD can absorb photons and generate electron-hole pairs (excitons) in the polymer. The excitons can then be separated into free electrons and holes, which can migrate to the surface of the MWCNTs due to the strong electron affinity of the nanotubes. The electrons on the MWCNTs can then react with electron-accepting species (e.g. oxygen, water, or organic pollutants) in the solution, leading to the degradation of pollutants or the generation of electrical current. Meanwhile, the holes created in the poly-TPD can react with electron-donating species (e.g. hydroxyl radicals), leading to the degradation of pollutants or the regeneration of the poly-TPD. To prevent the recombination of the electrons and holes, MWCNTs can act as electron sinks, effectively quenching the excitons and enhancing the photocatalytic efficiency. The nanocomposite system of poly-TPD/MWCNT can exhibit enhanced photocatalytic activity compared to the individual components due to the synergistic effects of the two materials. The photocatalysis efficiency and thus the charge transfer mechanism depends on several factors, including the energy offset between the MWCNTs and poly-TPD, the strength of the exciton-MWCNT coupling, and the presence of defects or impurities that can trap the exciton. The more addition of MWCNTs to poly-TPD resulted in a decrease in the energy band gap, which is supported by the data presented in Table 1. This decrease in the band gap led to a closer alignment of the lowest unoccupied molecular orbital (LUMO) and the highest occupied molecular orbital (HOMO) energy levels, facilitating the charges transfer within the system. MWCNTs also have a high surface area and can act as a scaffold for the poly-TPD, providing more reaction sites for the photocatalytic process and increase the efficiency of charge transfer [45]. The photocatalysis mechanism in nanocomposite systems like poly-TPD/MWCNT involves the efficient separation of excitons, charge transfer, and exciton quenching, which lead to enhanced photocatalytic activity. Such this mechanism has promising applications in various environmental and energy-related fields [46–48].

The Gaussian function can be used to deconvolute the PL curves into three vibronic bands. An example of a

deconvoluted emission curve is given in Fig. 5 inset for poly-TPD, and the results from the deconvolution of all PL curves are summarized in Table 2. The weight fraction of MWCNTs in the starting charge was seen to slightly increase the vibronic spacing energy from 0.154 to 0.160 eV, which is usually associated with a lower degree of chain disorder and a slight rise in π -electron delocalization [26]. Furthermore, as the MWCNT content increases, the stoke shift decreases until it reaches 2 wt%, and then there is a slight increase for ≥ 2.5 wt%, as indicated in Table 1. The change in the stoke shift value can be attributed to the charge transfer states, and as the MWCNT content increases, the stoke shift value also increases due to an increase in the number of charge transfer states [49]. The spectral intensity can be approximated by transitions between vibrational frequencies of the excited and ground electronic states, and this probability can be expressed as [50]:

$$I_{0 \rightarrow n} = \frac{e^{-S}}{n!} \quad (4)$$

where S is the Huang–Rhys factor (S-factor), which is related with conformational disorder [51]. As revealed in Table 2, the S-factor was slightly changed with increasing the MWCNTs content, confirming the good distribution of MWCNTs within the poly-TPD.

The parameters of the Stern–Volmer quenching constant (k_{SV}), fluorescence lifetime (τ) of excited poly-TPD in the presence of MWCNTs, photo-induced electron-transfer rate (k_{ET}), and bimolecular quenching rate (k_q) can be adjusted to further enhance the efficient charge transfer between the poly-TPD and MWCNTs [52].

The Stern–Volmer equation for collisional quenching can be expressed as [53]:

$$\frac{I_0}{I} = 1 + k_{SV}[Q] \quad (5)$$

where I and I_0 are the emission intensities in the presence and absence of quenching, respectively, and $[Q]$ is the quencher concentration. There is no change in the absorption spectrum of the poly-TPD when MWCNTs are added, meaning there are no ground-state interactions between the two. This suggests that the emission quenching is due to dynamic quenching [53], which is supported by the linear relationship between $\frac{I_0}{I}$ and $[Q]$ in the Stern–Volmer plot (Fig. 6) [54]. The slope of this linear fit gives a Stern–Volmer constant of 177 M^{-1} , which implies that 50% of fluorescence was quenched at a concentration of 5.65 mM. This homogeneous quenching may be due to good distribution of MWCNTs and sufficient coverage of poly-TPD on their surface.

The Stern–Volmer equation can be used to calculate the k_q and k_{ET} values for poly-TPD/MWCNTs hybrid thin films, where $\frac{I_0}{I}$ is replaced by $\frac{\tau_0}{\tau}$ [53]. This is demonstrated by Table 3, which shows that the fluorescence lifetime of poly-TPD decreases significantly with increasing quencher

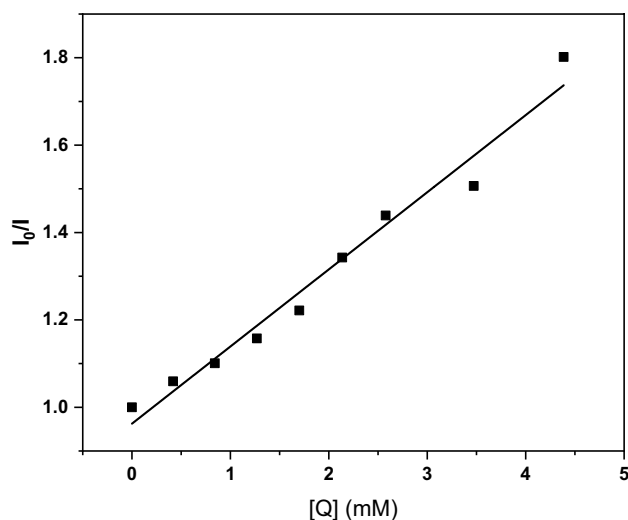


Fig. 6 Stern–Volmer plot for emission quenching of poly-TPD by MWCNTs

Table 2 Optical energy properties for poly-TPD/MWCNT composite

Content of MWCNT wt%	I_0/I	λ_{PL} 0–0 transition (nm)	λ_{PL} 0–1 transition (nm)	Stokes shift (nm)	Vibronic splitting (eV)	S-factor
0	1	419.0	442	53.7	0.154	0.451
0.5	1.059	419.0	442	53.0	0.154	0.450
1.0	1.101	419.2	442	53.2	0.153	0.450
1.5	1.157	419.0	442	53.0	0.154	0.452
2.0	1.221	419.4	442	53.4	0.151	0.452
2.5	1.342	422.5	446	56.5	0.155	0.445
3.0	1.439	422.6	447	56.6	0.160	0.449
5.0	1.506	422.6	447	56.6	0.160	0.453
10	1.802	422.6	447	56.6	0.160	0.450

Table 3 Photo-induced electron transport rate and lifetime values of poly-TPD/MWCNT nanocomposites

Content of MWCNT wt%	Concentration of MWCNTs [Q] (mM)	PL lifetime of poly-TPD (ns)	Photo-induced electron transport rate k_{ET} (S^{-1}) $\times 10^8$
0	0	1.36	–
0.5	0.42	1.28	0.44
1.0	0.84	1.23	0.74
1.5	1.27	1.17	1.16
2.0	1.70	1.11	1.63
2.5	2.14	1.01	2.52
3.0	2.58	0.94	3.23
5.0	3.47	0.90	3.72
10	4.39	0.75	5.89

(MWCNT) concentration. The pristine poly-TPD had a lifetime (τ_0) of 1.36 ns [55], and all composites had shorter lifetimes (τ) than this, indicating efficient charge transfer [56] and the absence of static quenching for the poly-TPD/MWCNTs [57].

The values of k_q and k_{ET} for poly-TPD/MWCNTs composites can be calculated using the following equations [58, 59]:

$$k_{ET} = \frac{1}{\tau} - \frac{1}{\tau_0} \quad (6)$$

$$k_{SV} = \tau_0 k_q \quad (7)$$

The k_q value of $1.30 \times 10^{11} \text{ M}^{-1} \text{ S}^{-1}$ is much higher than the minimum value for efficient quenching, $1 \times 10^{10} \text{ M}^{-1} \text{ S}^{-1}$ [53], which shows that the combination of poly-TPD and MWCNTs is successful. As more MWCNTs were added to the poly-TPD, the k_{ET} values increased from 0.44×10^8 to $5.89 \times 10^8 \text{ S}^{-1}$ (as seen in Table 3). This indicates that there is an enhancement in quenching efficiency and charge transfer in the composites with increasing MWCNT content. In other words, by adjusting the amount of MWCNTs, it is possible to control the k_{ET} values. A higher content of MWCNTs leads to a larger surface area and more defects, which increases the k_{ET} values and allows for more efficient optoelectrical devices to be made with poly-TPD/MWCNT composites.

4 Conclusion

The photophysical properties of the poly-TPD thin film were successfully altered by incorporation MWCNTs in varying ratios, without changing its structure. As the amount of MWCNTs increased, the refractive index, energy tail, stoke shift, and vibronic splitting also increased, while the energy band gap and steepness parameter decreased. The

incorporation of MWCNTs caused dynamic quenching in poly-TPD, as evidenced by the linear Stern–Volmer plot where 50% of fluorescence was quenched at a concentration of 5.65 mM. Additionally, the poly-TPD/MWCNTs nanocomposite thin films showed enhanced fluorescence lifetime, photo-induced electron-transfer rate, and bimolecular quenching rate, indicating effective charge transfer. The effectiveness charge transfer played unique role for enhancement optoelectrical devices based on poly-TPD/MWCNT nanocomposites.

Acknowledgements The author extend his appreciation to the Deputyship for Research & Innovation, “Ministry of Education in Saudi Arabia for funding this research work through the project no. (IFKSUOR3–024–1)”.

Author contributions BA did the following: conceptualization, methodology, formal analysis, investigation, writing—original draft preparation, writing—review and editing, and visualization.

Funding This research did not receive any specific grant from funding agencies in the public, commercial, or not-for-profit sectors.

Declarations

Conflict of interest The author declares that he has no known competing financial interests or personal relationships that could have appeared to influence the work reported in this paper.

References

1. A. Alsaad, Q.M. Al-Bataineh, A. Ahmad, I. Jum’h, N. Alaqdash, A. Bani-Salameh, Optical properties of transparent PMMA-PS/ZnO NPs polymeric nanocomposite films: UV-Shielding applications. *Mater. Res. Express* **6**(12), 126446 (2020)
2. A. Alsaad, A. Ahmad, A.R. Al Dairy, A.S. Al-anbar, Q.M. Al-Bataineh, Spectroscopic characterization of optical and thermal properties of (PMMA-PVA) hybrid thin films doped with SiO₂ nanoparticles. *Results Phys.* **19**, 103463 (2020)
3. S.B. Aziz, O.G. Abdullah, M. Brza, A.K. Azawy, D.A. Tahir, Effect of carbon nano-dots (CNDs) on structural and

- optical properties of PMMA polymer composite. *Results Phys.* **15**, 102776 (2019)
4. A. Rajeh, H. Ragab, M. Abutalib, Co doped ZnO reinforced PEMA/PMMA composite: structural, thermal, dielectric and electrical properties for electrochemical applications. *J. Mol. Struct.* **1217**, 128447 (2020)
 5. M. Hassan, K.R. Reddy, E. Haque, A.I. Minett, V.G. Gomes, High-yield aqueous phase exfoliation of graphene for facile nanocomposite synthesis via emulsion polymerization. *J. Colloid Interface Sci.* **410**, 43–51 (2013)
 6. D.W. Mosley, K. Auld, D. Conner, J. Gregory, X.-Q. Liu, A. Pedicini, D. Thorsen, M. Wills, G. Khanarian, E.S. Simon. (2008) Highperformance encapsulants for ultra high-brightness LEDs, In: *Light-emitting diodes: research, manufacturing, and applications XII*. SPIE. 221–228
 7. T. Nakamura, H. Fujii, N. Juni, N. Tsutsumi, Enhanced coupling of light from organic electroluminescent device using diffusive particle dispersed high refractive index resin substrate. *Opt. Rev.* **13**, 104–110 (2006)
 8. R.D. Allen, G.M. Wallraff, D.C. Hofer, R.R. Kunz, Photoresists for 193-nm lithography. *IBM J. Res. Dev.* **41**(1.2), 95–104 (1997)
 9. K.C. Krogman, T. Druffel, M.K. Sunkara, Anti-reflective optical coatings incorporating nanoparticles. *J. Nanotechnol.* **16**(7), S338 (2005)
 10. J.L. Regolini, D. Benoit, P. Morin, Passivation issues in active pixel CMOS image sensors. *Microelectron. Reliab.* **47**(4–5), 739–742 (2007)
 11. P. Tao, Y. Li, A. Rungta, A. Viswanath, J. Gao, B.C. Benicewicz, R.W. Siegel, L. Schadler, TiO₂ nanocomposites with high refractive index and transparency. *J. Mater. Chem.* **21**(46), 18623–18629 (2011)
 12. H.M. Zidan, E.M. Abdelrazek, A.M. Abdelghany, A.E. Tarabiah, Characterization and some physical studies of PVA/PVP filled with MWCNTs. *J. Mater. Res. Technol.* **8**(1), 904–913 (2019)
 13. S.H. Ryu, H.-B. Cho, S. Kim, Y.-T. Kwon, J. Lee, K.-R. Park, Y.-H. Choa, The effect of polymer particle size on three-dimensional percolation in core-shell networks of PMMA/MWCNTs nanocomposites: properties and mathematical percolation model. *Compos. Sci. Technol.* **165**, 1–8 (2018)
 14. A. Kumar, V. Kumar, M. Kumar, K. Awasthi, Synthesis and characterization of hybrid PANI/MWCNT nanocomposites for EMI applications. *Polym. Compos.* **39**(11), 3858–3868 (2018)
 15. N. Hota, N. Karna, K. Dubey, D. Tripathy, B. Sahoo, Effect of temperature and electron beam irradiation on the dielectric properties and electromagnetic interference shielding effectiveness of ethylene acrylic elastomer/millable polyurethane/SWCNT nanocomposites. *Eur. Polym. J.* **112**, 754–765 (2019)
 16. O. Breuer, U. Sundararaj, Big returns from small fibers: a review of polymer/carbon nanotube composites. *Polym. Compos.* **25**(6), 630–645 (2004)
 17. Y. Mamunya, A. Boudenne, N. Lebovka, L. Ibos, Y. Candau, M. Lisunova, Electrical and thermophysical behaviour of PVC-MWCNT nanocomposites. *Compos. Sci. Technol.* **68**(9), 1981–1988 (2008)
 18. H. Bao, X. Ruan, T.S. Fisher, Optical properties of ordered vertical arrays of multi-walled carbon nanotubes from FDTD simulations. *Opt. Express* **18**(6), 6347–6359 (2010)
 19. E. Lidorikis, A.C. Ferrari, Photonics with multiwall carbon nanotube arrays. *ACS Nano* **3**(5), 1238–1248 (2009)
 20. K.-I. Kim, D.-A. Kim, K.D. Patel, U.S. Shin, H.-W. Kim, J.-H. Lee, H.-H. Lee, Carbon nanotube incorporation in PMMA to prevent microbial adhesion. *Sci. Rep.* **9**(1), 4921 (2019)
 21. F. Hezam, A. Rajeh, O. Nur, M. Mustafa, Synthesis and physical properties of spinel ferrites/MWCNTs hybrids nanocomposites for energy storage and photocatalytic applications. *Phys. B Condens. Matter.* **596**, 412389 (2020)
 22. M. Morsi, A. Rajeh, A. Al-Muntaser, Reinforcement of the optical, thermal and electrical properties of PEO based on MWCNTs/Au hybrid fillers: nanodielectric materials for organoelectronic devices. *Compos. B Eng.* **173**, 106957 (2019)
 23. E.Y. Malikov, M.B. Muradov, O.H. Akperov, G.M. Eyvazova, R. Puskás, D. Madarász, L. Nagy, Á. Kukovecz, Z. Kónya, Synthesis and characterization of polyvinyl alcohol based multiwalled carbon nanotube nanocomposites. *Phys. E Low-Dimens. Syst. Nanostruct.* **61**, 129–134 (2014)
 24. M.I. Delgado-Rosero, N.M. Jurado-Meneses, R. Uribe-Kaffure, Composite Polymer Electrolytes based on (PEO) 4CF3COOLi and multi-walled Carbon Nanotube (MWCNT). *Polymers* **15**(1), 49 (2023)
 25. M. Kók, M.E. Pekdemir, E. Öner, M. Coşkun, S. Hekim, MWCNT nanocomposite films prepared using different ratios of PVC/PCL: combined FT-IR/DFT, thermal and shape memory properties. *J. Mol. Struct.* **18**, 134989 (2023)
 26. D. Ginger, N. Greenham, Charge separation in conjugated-polymer/nanocrystal blends. *Synth. Met.* **101**(1–3), 425–428 (1999)
 27. K. Hazarika, H.R. Thakur, J.C. Dutta, Fabrication and characterization of different polymer doped CNT nanocomposites for creatinine detection. *Mater. Today Proc.* (2023). <https://doi.org/10.1016/j.matpr.2023.01.032>
 28. F. Zhou, Y. Wang, W. Wu, T. Jing, S. Mei, Y. Zhou, Synergetic signal amplification of multi-walled carbon nanotubes-Fe₃O₄ hybrid and trimethyloctadecylammonium bromide as a highly sensitive detection platform for tetrabromobisphenol A. *Sci. Rep.* **6**(1), 1–12 (2016)
 29. N. Juhari, W.H.A. Majid, Z.A. Ibrahim, Structural and optical studies of MEH-PPV using two different solvents prepared by spin coating technique. *Solid State Sci. Technol.* **15**(1), 141–146 (2007)
 30. B.A. Al-Asbahi, A.A. Alanezi, M.S. AlSalhi, Photophysical characteristics of multicolor emitting MDMO-PPV–DMP/ZnO hybrid nanocomposites. *Molecules* **27**(3), 843 (2022)
 31. K. Bazaka, M.V. Jacob, Effects of iodine doping on optoelectronic and chemical properties of polyterpenol thin films. *Nanomaterials* **7**(1), 11 (2017)
 32. A. Petrella, M. Tamborra, M.L. Curri, P. Cosma, M. Striccoli, P.D. Cozzoli, A. Agostiano, Colloidal TiO₂ nanocrystals/MEH-PPV nanocomposites: photo (electro) chemical study. *J. Phys. Chem. B* **109**(4), 1554–1562 (2005)
 33. A.A. Zainudin, Y.W. Fen, N.A. Yusof, N.A.S. Omar, Structural, optical and sensing properties of ionophore doped graphene based bionanocomposite thin film. *Optik* **144**, 308–315 (2017)
 34. Y.-H. Chen, C.-H. Ho, Temperature dependence of direct and indirect band gaps of Bi₁₃I₂S₁₈ hexagonal rod crystals. *Mater. Chem. Phys.* **206**, 71–75 (2018)
 35. B.H. Rabee, B.A. Al-Kareem, Study of optical properties of (PMMA-CuO) nanocomposites. *Int. J. Sci. Res.* **5**, 879–883 (2016)
 36. S.B. Aziz, Modifying poly (vinyl alcohol) (PVA) from insulator to small-bandgap polymer: a novel approach for organic solar cells and optoelectronic devices. *J. Electron. Mater.* **45**(1), 736–745 (2016)
 37. S. Prasher, M. Kumar, S. Singh, Electrical and optical properties of O⁶⁺ ion Beam-Irradiated polymers. *Int. J. Polym. Anal. Character.* **19**(3), 204–211 (2014)
 38. F. Urbach, The long-wavelength edge of photographic sensitivity and of the electronic absorption of solids. *Phys. Rev.* **92**(5), 1324 (1953)
 39. N. Tigau, V. Ciupina, G. Prodan, Structural, optical and electrical properties of Sb₂O₃ thin films with different thickness. *J. Optoelectron. Adv. Mater.* **8**(1), 37 (2006)
 40. J. Zou, P. Le Rendu, I. Musa, S.-H. Yang, Y. Dan, C.T. That, T. Nguyen, Investigation of the optical properties of polyfluorene/

- ZnO nanocomposites. *Thin Solid Films* **519**(12), 3997–4003 (2011)
41. B.A. Al-Asbahi, A.A. Alanezi, M.S. AlSalhi, Materials, enhancing photophysical properties of MDMO-PPV-DMP conjugated polymer via incorporation anatase titania nanoparticles. *J. Inorg. Organomet. Polym.* **32**(9), 3556–3563 (2022)
 42. V. Dimitrov, S. Sakka, Linear and nonlinear optical properties of simple oxides. II. *J. Appl. Phys.* **79**(3), 1741–1745 (1996)
 43. A. Abdelghany, M. Morsi, A. Abdelrazek, M. Ahmed, Role of silica nanoparticles on structural, optical and morphological properties of poly (vinyl chloride-co-vinyl acetate-co-2-hydroxypropyl acrylate) copolymer. *Silicon* **10**, 519–524 (2018)
 44. S.-H. Yang, P. Le Rendu, T.P. Nguyen, C.-S. Hsu, Fabrication of MEH-PPV/SiO₂ and MEH-PPV/TiO₂ nanocomposites with enhanced luminescent stabilities. *Rev. Adv. Mater. Sci.* **15**(2), 144–149 (2007)
 45. Y. Yan, H. Sun, L. Zhang, J. Zhang, J. Mu, S.-Z. Kang, Effect of multiwalled carbon nanotubes on the photocatalytic degradation of methyl orange in aqueous solution under visible light irradiation. *J. Dispers. Sci. Technol.* **32**(9), 1332–1336 (2011)
 46. J. Zhang, B. Zhu, L. Zhang, J. Yu, Femtosecond transient absorption spectroscopy investigation on electron transfer mechanism in photocatalysis. *Chem. Commun.* **59**(1), 688–699 (2023)
 47. J. Zhang, L. Zhang, W. Wang, J. Yu, In situ irradiated X-ray photoelectron spectroscopy investigation on electron transfer mechanism in S-scheme photocatalyst. *J. Phys. Chem. Lett.* **13**(36), 8462–8469 (2022)
 48. L. Wang, J. Zhang, H. Yu, I.H. Patir, Y. Li, S. Wageh, A.A. Al-Ghamdi, J. Yu, Dynamics of photogenerated charge carriers in inorganic/organic S-scheme heterojunctions. *J. Phys. Chem. Lett.* **13**(21), 4695–4700 (2022)
 49. U. Kumar, S. Upadhyay, P.A. Alvi, Study of reaction mechanism, structural, optical and oxygen vacancy-controlled luminescence properties of Eu-modified Sr₂SnO₄ ruddlesden popper oxide. *Phys. B Condens. Matter.* **604**, 412708 (2021)
 50. H. Bäessler, B. Schweitzer, Site-selective fluorescence spectroscopy of conjugated polymers and oligomers. *Acc. Chem. Res.* **32**(2), 173–182 (1999)
 51. J. Blatchford, S. Jessen, L.-B. Lin, T. Gustafson, D.-K. Fu, H.-L. Wang, T. Swager, A. MacDiarmid, A. Epstein, Photoluminescence in pyridine-based polymers: role of aggregates. *J. Phys. Rev. B.* **54**(13), 9180 (1996)
 52. B.A. Al-Asbahi, M.H.H. Jumali, R. Al-Gaashani, Efficient charge transfer mechanism in Polyfluorene/ZnO nanocomposite thin films. *J. Nanomater.* **2014**, 87–87 (2014)
 53. J. Lakowicz, *Principles of Fluorescence Spectroscopy*, 2nd edn. (Kluwer Academic, New York, 1999)
 54. B.A. Al-Asbahi, S.M. Qaid, A.S. Aldwayyan, Effect of donor-acceptor concentration ratios on non-radiative energy transfer in zero-dimensional Cs₄PbBr₆ perovskite/MEH-PPV nanocomposite thin films. *Polymers* **12**(2), 444 (2020)
 55. X. Zhang, H. Dai, J. Zhao, S. Wang, X. Sun, All-solution processed composite hole transport layer for quantum dot light emitting diode. *Thin Solid Films* **603**, 187–192 (2016)
 56. Y.-Y. Lin, T.-H. Chu, C.-W. Chen, W.-F. Su, Improved performance of polymer/TiO₂ nanorod bulk heterojunction photovoltaic devices by interface modification. *Appl. Phys. Lett.* **92**(5), 40 (2008)
 57. T. Vats, S.N. Sharma, M. Kumar, M. Kar, K. Jain, V. Singh, B. Mehta, A. Narula, Comparison of photostability, optical and structural properties of TiO₂/conjugated polymer hybrid composites prepared via different methods. *Thin Solid Films* **519**(3), 1100–1105 (2010)
 58. F. Ricchelli, Photophysical properties of porphyrins in biological membranes. *J. Photochem. Photobiol. B Biol.* **29**(2–3), 109–118 (1995)
 59. J. Zimmermann, J. Von Gersdorff, H. Kurreck, B. Röder, Determination of the electron transfer parameters of a covalently linked porphyrin-quinone with mesogenic substituents—optical spectroscopic studies in solution. *J. Photochem. Photobiol. B Biol.* **40**(3), 209–217 (1997)

Publisher's Note Springer Nature remains neutral with regard to jurisdictional claims in published maps and institutional affiliations.

Springer Nature or its licensor (e.g. a society or other partner) holds exclusive rights to this article under a publishing agreement with the author(s) or other rightsholder(s); author self-archiving of the accepted manuscript version of this article is solely governed by the terms of such publishing agreement and applicable law.